EarthArXiv Coversheet

Robert Kostynick[1], Julia Prata[1], Jesse Bower[2], and Claire Masteller[1]

[1]Earth, Environmental, and Planetary Sciences, Washington University in St. Louis, St. Louis, MO, USA

[2]Department of Civil & Environmental Engineering, Utah State University, Logan, UT, USA

cmasteller@wustl.edu

This pre-print is in review at *Geology* and has undergone no rounds of peer-review.

Slope-dependent riverbed strengthening and the evolution of the threshold for motion in gravel-bed rivers

Robert Kostynick[1], Julia Prata[1], Jesse Bower[2], and Claire Masteller[1]

[1]Deptartment of Earth, Environmental, and Planetary Sciences, Washington University in St. Louis, St. Louis, MO, USA

[2]Department of Civil and Environmental Engineering, Utah State University, Logan, UT, USA

ABSTRACT

The threshold for motion exerts a fundamental control on sediment transport, channel morphology, and fluvial erosion. While channel slope and flow history are known to influence entrainment thresholds in gravel-bed rivers, their interaction has not been explored. We investigate how channel slope modulates riverbed strengthening during low-flow periods. Flume experiments were conducted across slopes spanning more than an order of magnitude (S=5–70 mm/m) with hydraulic forcing scaled relative to slope-specific entrainment thresholds. Across all slopes, sediment flux decreased with increasing conditioning time, indicating progressive riverbed strengthening. Strengthening rates increased strongly with slope, reflecting more effective stabilization by low flows. At steep slopes, reduced hydrodynamic lift forces may combine with ongoing granular rearrangement during low flows to progressively stabilize the bed, increasing grain resistance to entrainment. These results demonstrate that slope exerts a strong control on riverbed recovery following floods. Because strengthening rates scale predictably with channel gradient, slope may provide a first-order parameter for predicting flow-history-driven evolution of entrainment thresholds in sediment transport models, with

implications for erosion rates, channel form, and the distribution of geomorphic work across watersheds.

INTRODUCTION

River erosion shapes landscapes by carving valleys (Brocard and van der Beek, 2006), organizing drainage networks (Gasparini et al., 2004), and regulating the delivery of water and sediment to oceans (Syvitski et al., 2005). In gravel-bed rivers, sediment transport controls both the pace of erosion and channel morphology (Parker, 1978; Phillips et al., 2022), influencing flood hazards, aquatic habitat structure, and water quality. Despite the central role of sediment transport in shaping rivers and landscapes, accurate predictions of bedload flux remain challenging due to the complex coupling between turbulent flow and granular riverbeds (Jerolmack and Daniels, 2019; Hosseiny et al., 2023). Addressing this challenge requires a deeper understanding of the physical processes that govern how rivers erode their beds.

A fundamental control on sediment transport and fluvial erosion is the threshold for sediment motion, which defines the flow conditions above which rivers can mobilize the riverbed. When flows exceed this threshold, bedload transport conveys sediment downstream. This redistribution of sediment along river channels can, in turn, alter channel morphology. Further, once the entrainment threshold is exceeded, sediment transport intensity and grain impact energies increase rapidly, influencing bedrock erosional efficiency (Sklar and Dietrich, 2004; Masteller et al., 2024). In this way, the threshold for motion controls which floods are most effectively translated into geomorphic work, governing the portion of the discharge distribution that contributes to landscape change (DiBiase and Whipple, 2011). The threshold for motion also underpins channel geometry such that rivers adjust their width, depth, and slope so that at bankfull conditions, flows only slightly exceed the threshold for motion, allowing

sediment to be transported downstream without significant bank erosion (Parker, 1978; Phillips et al., 2022).

The threshold for motion is commonly represented as critical Shields stress, τ_c^*, a nondimensional parameter normalizing boundary shear stress by sediment grain size (Shields, 1936). In many applications, critical Shields stress is held constant, with bedload flux formulae often assuming a specific value of τ_c^* (e.g. Wong and Parker, 2006). Early data compilations suggested that τ_c^* occupies a narrow range (0.03–0.1; e.g., Buffington and Montgomery, 1997). However, subsequent work has shown that the threshold for motion can vary widely across rivers and through time. This variability arises from changes in hydraulic conditions (Lamb et al., 2017), riverbed structure (Kirchner et al., 1990; Whitfield et al., 2025), sediment supply (Yager et al., 2012; Johnson, 2016), grain exposure and protrusion (Masteller and Finnegan, 2017; Yager et al., 2018; Hodge et al., 2019), and even biological activity (Albertson et al., 2014; Masteller et al., 2015).

Channel slope exerts a strong control on entrainment thresholds. Steeper slopes produce shallower flows and greater relative roughness, modifying turbulent structures and grain-scale forces acting on the bed (Mueller et al., 2005; Lamb et al., 2008, 2017; Prancevic and Lamb, 2015). As a result, τ_c^* systematically increases with channel slope despite greater downstream gravitational forcing. Masteller et al. (in review) highlights that this relationship is reflected in bankfull channel geometry within individual river systems, with steep headwaters organizing to reflect higher bankfull Shields stresses relative to low-slope downstream reaches.

Riverbed erosion thresholds also evolve through time. Numerous studies have demonstrated that τ_c^* is sensitive to the history of recent flows, reflecting a “memory” of the magnitude and duration of previous hydraulic forcing. Periods of low flow allow grains to

rearrange locally, reducing protrusion and increasing τ_c^* between transport events (Ockelford and Haynes, 2013; Masteller and Finnegan, 2017). Subsequent high-magnitude floods can disrupt this strengthened bed structure by mobilizing grains and resetting τ_c^* (Turowski et al., 2009; Masteller et al., 2019). Building on these observations, Masteller et al. (2025) developed a model that captures the temporal evolution of τ_c^* by weighing the competing effects of riverbed strengthening and weakening as a function of flow history. These history-dependent thresholds are also expressed in channel geometry, with rivers experiencing lower bankfull intermittency tending to be narrower than those with high intermittency (Phillips et al., 2024).

Although both slope and flow history exert strong influences on τ_c^*, how these effects interact has never been directly explored. As a result, we lack a mechanistic understanding of how channel slope influences the rate and magnitude of riverbed strengthening during low flows. This knowledge gap limits our ability to predict how sediment transport thresholds and by extension, river morphology varies along river networks.

EXPERIMENTAL DESIGN AND HYDRAULIC SCALING

To investigate how channel slope influences riverbed strengthening during low flows, we conducted a series of flume experiments in a 0.4 m wide, 4.5 m long tilting flume. The upstream end of the flume is mounted on hydraulic cylinders that allow the flume to be adjusted over a wide range of slopes. We completed experiments at four slopes spanning over an order of magnitude: S=5, 25, 50, and 70 mm/m. The channel bed consisted of a gravel mixture with median grain size D_{50}=7.4 mm and a lognormal grain-size distribution, selected to approximate natural gravel-bed rivers and facilitate comparison with previous experiments (Masteller and Finnegan, 2017). Sediment exiting the flume was captured in a downstream basket to quantify bedload transport rates.

To ensure that all runs experienced equivalent flow histories despite large differences in channel slope, hydraulic forcing was scaled relative to τ_c^* specific to each slope, rather than applying identical discharges or Shields stresses across experiments. Sediment transport rating curves were constructed from a series of short (3 min) transport runs spanning a range of flow depths (Fig. 1A). Slope-specific reference Shields stress, τ_{ref}^*, was then estimated from each rating curve using a reference dimensionless transport rate, q_s^* = 0.08 (e.g. Prancevic and Lamb, 2015; Fig. 2B). τ_{ref}^* increases systematically with channel slope, ranging from $\tau_{ref}^* = 0.012$ to 0.063, and is well described by $\tau_{ref}^* = 0.30S^{0.61} (R^2 = 0.99)$.

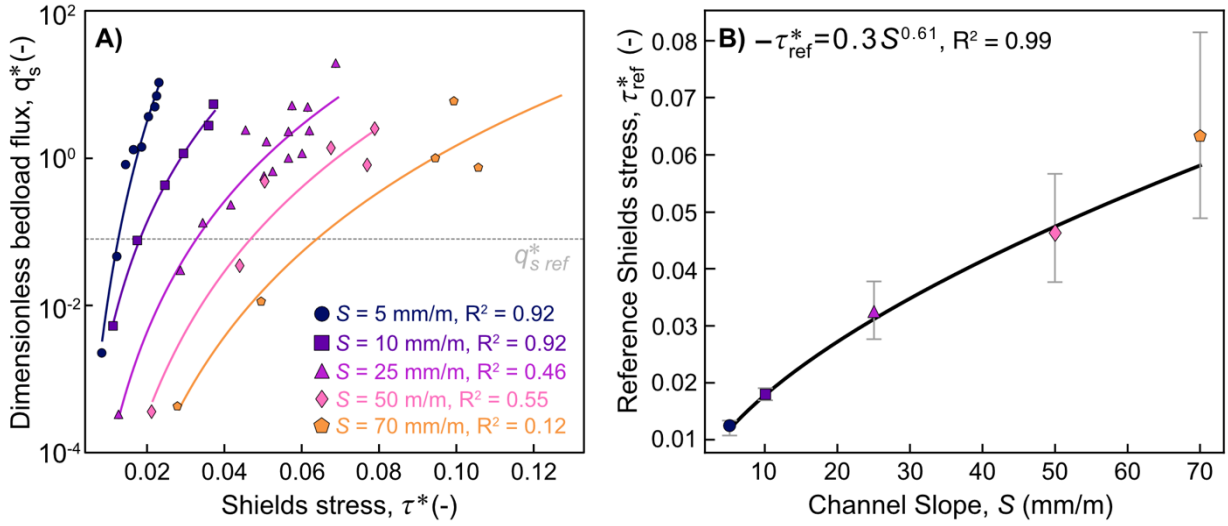

Figure 1. A) sediment transport rating curves; B) Estimates of τ_{ref}^* with channel slope; error bars represent the 75% confidence interval.

For each slope, low-flow conditioning and above-threshold transport flows were prescribed as fixed fractions of τ_{ref}^*, with conditioning flows targeting $0.75\tau_{ref}^*$ and transport floods, $1.2\tau_{ref}^*$. By scaling conditioning and transport flows, experiments conducted at different slopes experienced near identical flow histories relative to their slope-specific entrainment thresholds, allowing for direct comparison.

Each experiment had three stages designed to isolate the effects of antecedent low flows on sediment mobility. First, the bed was manually mixed, screeded, and leveled to remove any armoring and bed structure, ensuring the most reproducible initial condition possible. The bed was then subjected to a conditioning flow ($0.75\tau^*_{ref}$) lasting between 1 and 300 minutes. Following conditioning, a short-duration transport flood (5 min) was applied to mobilize sediment and drive bedload transport. For shorter conditioning times where transport rates were more variable, replicate runs were performed and mean sediment flux is reported.

SLOPE-DEPENDENT RIVERBED STRENGTHENING

Sediment flux, q_s (kg/m/s), following the transport flood decreases systematically with increasing conditioning time across all experimental slopes with significant negative correlations (Spearman's ρ: -0.71 to -0.88, all p-values < 0.047). Across all experimental slopes, longer antecedent low flows produce progressively lower bedload transport rates. After 300 minutes of conditioning, average bedload flux decreases by a factor of 4 at the lowest slopes and to over an order of magnitude at the steepest slopes. Reductions in flux are most rapid in early stages of conditioning, with transport rates plateauing at minimum values for low flows exceeding 100 minutes.

To quantify the rate of riverbed strengthening, we fit a power-law to each slope-specific dataset of the form $q_s = \alpha t^{-\zeta}$, where t is low flow conditioning time and ζ is the riverbed strengthening exponent. Larger values of ζ reflect more efficient strengthening. To facilitate comparison across slopes and with previous experiments from Masteller and Finnegan (2017) (S=8 mm/m), q_s was normalized using the data-derived α values for each slope set to account for differences in initial bed conditions and uncertainties in threshold estimates (Fig. 2). This normalization affects only the coefficient of the flux-time relationship and does not influence the

value of ζ or the goodness-of-fit with conditioning time. Across experiments, flux is well described by power-law fits with R^2=0.81-0.97. Goodness-of-fit metrics are reduced for steep slopes, where shallow flows introduce greater uncertainty in estimates of Shields stress and experimental scaling.

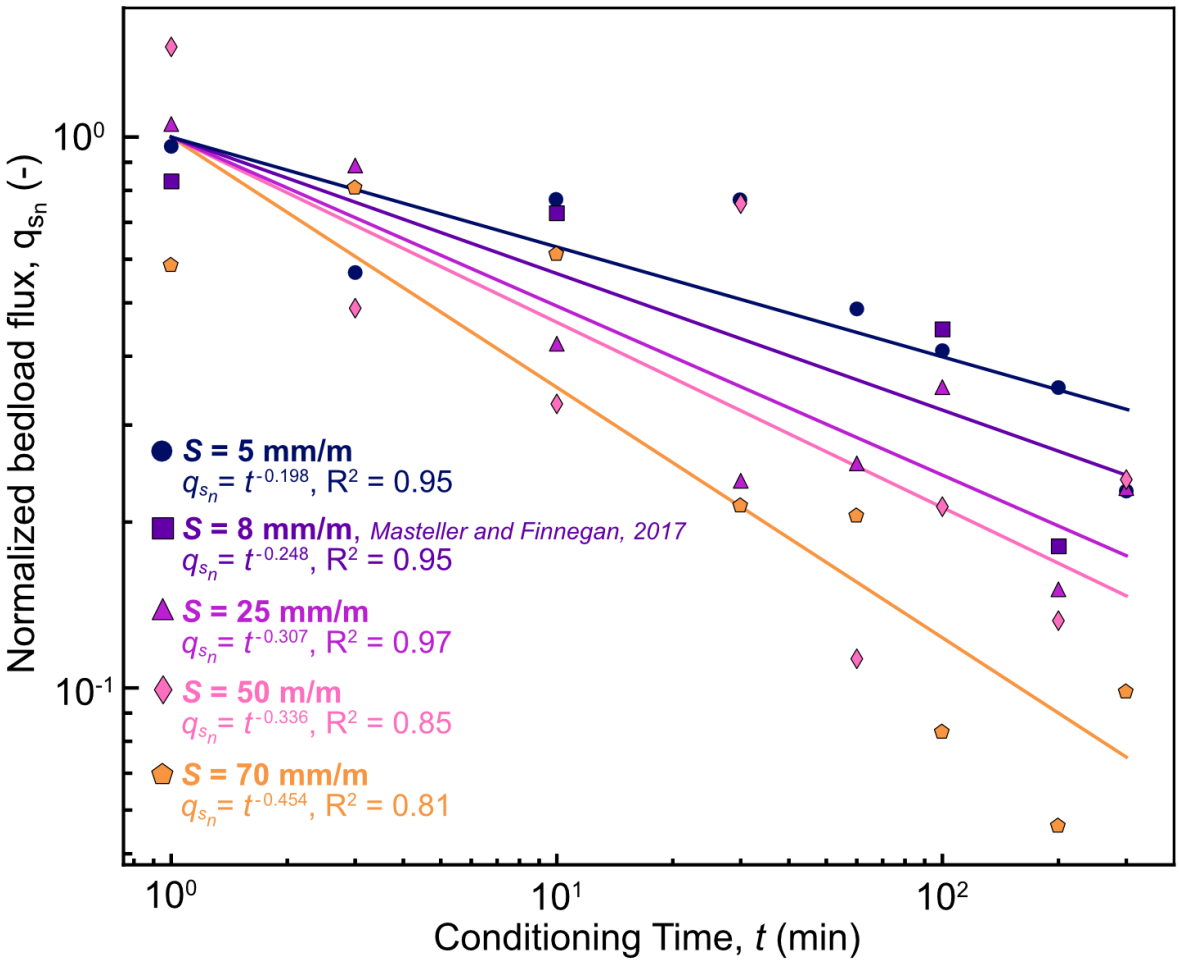

Figure 2. Normalized sediment flux, q_{s_n}, with conditioning time for each experimental slope and data from Masteller and Finnegan (2017) with best-fit power laws.

ζ increases systematically with slope, indicating that riverbeds strengthen more rapidly at steeper slopes (Fig. 3). For the lowest slope S=5 mm/m, ζ=0.198 (R^2=0.95), compared to a

ζ=0.454 (R^2=0.81) at S=70 mm/m. These differences in ζ imply large contrasts in the degree of transport reduction across our experiments. Over 300 minutes of conditioning, ζ predicts only a ~2-fold reduction in flux at S=0.005, whereas the highest-slope ζ predicts over an order-of-magnitude (~13-fold) reduction. These results highlight that even under near identical flow histories, riverbeds at steeper slopes stabilize far more efficiently during low flow. Indeed, ζ scales systematically with channel slope following a power-law relationship, $\zeta = 0.87S^{0.28}$ (R^2=0.90; Fig. 3). Strengthening exponents derived from previously published experiments conducted in a different flume (Masteller and Finnegan, 2017) fall directly along the trend defined by our experimental data. The remarkably strong fit of this relationship indicates that the rate at which riverbeds strengthen during low flows varies systematically and predictably with channel slope.

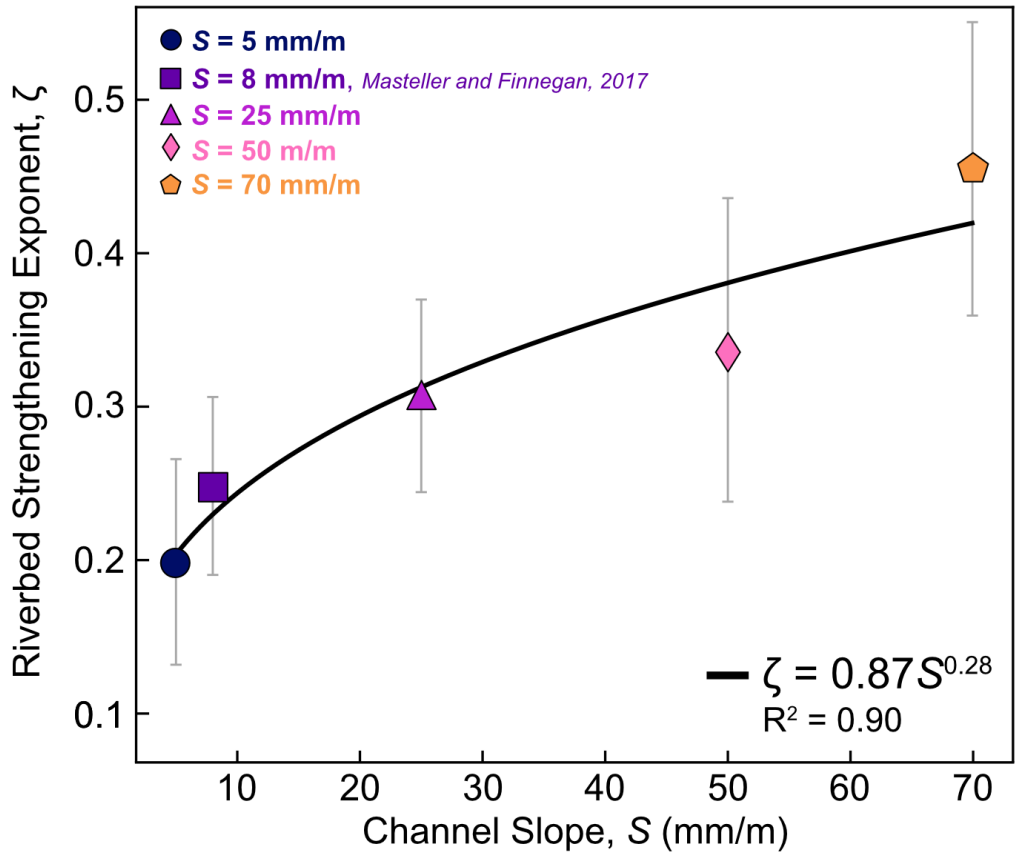

Figure 3. Riverbed strengthening exponent, ζ, as a function of slope. Error bars denote ±1 standard deviation uncertainty associated with the power-law fits used to estimate ζ.

IMPLICATIONS FOR RIVER PROCESS AND FORM

Our experiments provide the first demonstration that channel slope has a strong influence on flow-history-driven evolution of entrainment thresholds. Although riverbed strengthening during low flow has been documented in laboratory and field studies (e.g., Masteller and Finnegan, 2017; Masteller et al., 2019), our results demonstrate that strengthening rate varies systematically with channel slope. Riverbeds at steeper slopes stabilize more rapidly during low flows, even when hydraulic forcing is scaled relative to slope-specific entrainment thresholds. The strengthening exponent, ζ, varies predictably with slope, suggesting that channel gradient governs the rate at which riverbeds recover stability after floods by influencing the physical processes that stabilize the bed surface. This finding is particularly significant because it implies that models describing the evolution of τ_c^* as a function of flow history (e.g., Masteller et al., 2025) may be parameterized across river networks using channel slope as a predictor of relative strengthening rates.

Sediment flux in gravel-bed rivers is often strongly influenced by the most highly protruding grains on the bed surface, which are preferentially exposed to hydrodynamic forces and therefore more susceptible to entrainment (Yager et al., 2018; Hodge et al., 2019). Previous work has also shown that the number of protruding grains can decrease during periods of low-flow conditioning as grains reorganize into more stable configurations (Masteller and Finnegan, 2017). These observations suggest that protrusion may provide an important grain-scale control on how riverbeds strengthen between floods. However, more work is needed to determine whether the same population of highly protruding grains governs sediment transport across all

channel slopes, or if effective protrusion thresholds that influence mobility shift with channel gradient.

One possible mechanism for enhanced strengthening at steep slopes involves the interaction of grain-scale rearrangement and shallow-flow hydraulics. Lower relative submergence, or the ratio of flow depth to grain size, increases grain exposure to flow, strengthening the interaction between sediment grains and turbulent fluctuations. During low-flow conditioning, near-threshold stresses acting on exposed grains, paired with a greater downslope gravitational force, may more effectively pivot grains into pockets and more stable configurations. During floods, shallow-flow hydraulics may further enhance bed stability. At steep slopes, flow depths approach grain-scale roughness heights ($\frac{h}{D_{50}} \lesssim 1$) and turbulent wakes around grains can reduce or even reverse lift forces (Lamb et al., 2017). Under these conditions, high protruding grains become more difficult to dislodge. Together, these processes may combine to cause riverbeds at steeper slopes to stabilize more efficiently in response to the same flow history.

Sediment entrainment at steep slopes may also become increasingly controlled by intermittent turbulence or particle collisions. If beds at steep slopes are more stable overall, grains may remain immobile under typical boundary shear stresses and only become mobilized primarily during brief, high-magnitude fluctuations in flow. Turbulent sweeps and bursts can generate large instantaneous forces capable of entraining grains that would otherwise remain stable (e.g., Diplas et al., 2008). Under such conditions, sediment transport may become dominated by rare stochastic events rather than sustained hydraulic forcing, potentially allowing grains across a broader range of protrusions to contribute to sediment flux. Alternatively, collisions may drive collective entrainment (e.g. Lee and Jerolmack, 2018), where impacts

mobilize neighboring particles largely independent of their protrusion. Greater overall bed stability at steep slopes may therefore shift sediment transport toward rare, stochastic events rather than sustained forcing acting on the most exposed grains.

CONCLUSIONS

Our results show that slope exerts a previously unrecognized control on riverbed resilience and recovery following disturbance by floods. If steep channels recover bed stability more rapidly during intervening low-flow periods, their beds spend a greater fraction of time in a strengthened state characterized by elevated τ_c^*. This could systematically alter how geomorphic work is distributed across rivers, shifting the floods that accomplish the most sediment transport and bedrock erosion toward larger, less frequent events in steep channel headwaters. Such shifts may drive headwater reaches to organize around bankfull geometries that reflect elevated τ_c^* and longer bankfull recurrence intervals. Patterns consistent with this idea have been observed in mountain rivers, where bankfull channel morphology in headwaters indicates reduced mobility relative to low-gradient downstream reaches (Mueller et al., 2005; Masteller et al.). As such, the joint impact of channel slope and flow-history on τ_c^* may give rise to distinct, catchment-specific scaling relationships in bankfull hydraulic geometry across river networks (Kostynick et al., 2026). Additional work is needed to disentangle transient strengthening effect from the broader influence of slope on sediment entrainment thresholds and stable channel form. Our results reveal that channel gradient regulates how rivers retain and express the memory of past flows through evolving entrainment thresholds. Incorporating slope-dependent flow-history-effects into sediment transport and incision models can help to improve predictions of how river networks respond to and integrate hydroclimatic variability.

ACKNOWLEDGMENTS

Research was supported by the NSF Division of Earth Sciences EAR-2220504 and EAR-2220505.

REFERENCES CITED

Albertson, L.K., Sklar, L.S., Pontau, P., Dow, M., and Cardinale, B.J., 2014, A mechanistic model linking insect (Hydropsychidae) silk nets to incipient sediment motion in gravel-bedded streams: Journal of Geophysical Research: Earth Surface, v. 119, p. 1833–1852, doi:10.1002/2013JF003024.

Brocard, G.Y., and van der Beek, P.A., 2006, Influence of incision rate, rock strength, and bedload supply on bedrock river gradients and valley-flat widths: Field-based evidence and calibrations from western Alpine rivers (southeast France), *in* Tectonics, Climate, and Landscape Evolution, Geological Society of America, doi:10.1130/2006.2398(07).

Buffington, J.M., and Montgomery, D.R., 1997, A systematic analysis of eight decades of incipient motion studies, with special reference to gravel-bedded rivers: Water Resources Research, v. 33, p. 1993–2029, doi:https://doi.org/10.1029/96WR03190.

DiBiase, R.A., and Whipple, K.X., 2011, The influence of erosion thresholds and runoff variability on the relationships among topography, climate, and erosion rate: Journal of Geophysical Research, 116(F4), F04036.

Gasparini, N.M., Tucker, G.E., and Bras, R.L., 2004, Network-scale dynamics of grain-size sorting: implications for downstream fining, stream-profile concavity, and drainage basin morphology: Earth Surface Processes and Landforms, v. 29, p. 401–421, doi:10.1002/esp.1031.

Hodge, R.A., Voepel, H., Leyland, J., Sear, D.A., and Ahmed, S., 2019, X-ray computed tomography reveals that grain protrusion controls critical shear stress for entrainment of fluvial gravels: Geology, v. 48, p. 149–153, doi:10.1130/G46883.1.

Hosseiny, H., Masteller, C.C., Dale, J.E., and Phillips, C.B., 2023, Development of a machine learning model for river bed load: Earth Surface Dynamics, v. 11, p. 681–693, doi:10.5194/esurf-11-681-2023.

Jerolmack, D.J., and Daniels, K.E., 2019, Viewing Earth's surface as a soft-matter landscape: Nature Reviews Physics, v. 1, p. 716–730, doi:10.1038/s42254-019-0111-x.

Johnson, J.P.L., 2016, Gravel threshold of motion: a state function of sediment transport disequilibrium? Earth Surface Dynamics, v. 4, p. 685–703, doi:10.5194/esurf-4-685-2016.

Kirchner, J.W., Dietrich, W.E., Iseya, F., and Ikeda, H., 1990, The variability of critical shear stress, friction angle, and grain protrusion in water-worked sediments: Sedimentology, v. 37.

Kostynick, R.P., Phillips, C.B., and Masteller, C.C., 2026, High-Resolution Channel Geometry Reveals Contrasting Styles of Gravel River Adjustment: Geophysical Research Letters, doi:10.1029/2025GL118412.

Lamb, M.P., Brun, F., and Fuller, B.M., 2017, Direct measurements of lift and drag on shallowly submerged cobbles in steep streams: Implications for flow resistance and sediment transport: Water Resources Research, v. 53, p. 7607–7629, doi:10.1002/2017WR020883.

Lamb, M.P., Dietrich, W.E., and Venditti, J.G., 2008, Is the critical Shields stress for incipient sediment motion dependent on channel-bed slope? Journal of Geophysical Research, v. 113, p. F02008, doi:10.1029/2007JF000831.

Lee, D.B., and Jerolmack, D., 2018, Determining the scales of collective entrainment in collision-driven bed load: Earth Surface Dynamics, v. 6.

Masteller, C.C., Chandler, H., and Bower, J., 2024, The Fluvial Battering Ram: Collisional Experiments Reveal the Importance of Particle Impact Energies on Bedrock Erosional Efficiency: Geophysical Research Letters, v. 51, p. e2024GL109533, doi:10.1029/2024GL109533.

Masteller, C.C., and Finnegan, N.J., 2017, Interplay between grain protrusion and sediment entrainment in an experimental flume: Journal of Geophysical Research: Earth Surface, v. 122, p. 274–289, doi:10.1002/2016JF003943.

Masteller, C.C., Finnegan, N.J., Turowski, J.M., Yager, E.M., and Rickenmann, D., 2019, History-Dependent Threshold for Motion Revealed by Continuous Bedload Transport Measurements in a Steep Mountain Stream: Geophysical Research Letters, v. 46.

Masteller, C.C., Finnegan, N.J., Warrick, J.A., and Miller, I.M., 2015, Kelp, cobbles, and currents: Biologic reduction of coarse grain entrainment stress: Geology, v. 43, p. 543–546, doi:10.1130/G36616.1.

Masteller, C.C., Johnson, J.P.L., Rickenmann, D., and Turowski, J.M., 2025, Modeling memory in gravel-bed rivers: a flow-history-dependent relation for evolving thresholds of motion: Earth Surface Dynamics, v. 13, p. 593–605, doi:10.5194/esurf-13-593-2025.

Masteller, C.C., Phillips, C.B., Kostynick, R.P., Castejon-Villalobos, J.F., Lopez, C.G., Shallue, M.K., Bower, J., and Sigman, A. Tracking the trajectory of alluvial channel adjustment along a river's profile:, https://www.authorea.com/users/721760/articles/1389848-tracking-the-trajectory-of-alluvial-channel-adjustment-along-a-river-s-profile?commit=6b8c3cfa541fa066011c7bd093ab3cbce4fe7c62 (accessed March 2026).

Mueller, E.R., Pitlick, J., and Nelson, J.M., 2005, Variation in the reference Shields stress for bed load transport in gravel-bed streams and rivers: Water Resources Research, v. 41, p. W04006, doi:10.1029/2004WR003692.

Ockelford, A.-M., and Haynes, H., 2013, The impact of stress history on bed structure: Earth Surface Processes and Landforms, v. 38, p. 717–727, doi:https://doi.org/10.1002/esp.3348.

Parker, G., 1978, Self-formed straight rivers with equilibrium banks and mobile bed. Part 2: The gravel river. Journal of Fluid Mechanics, v. 89, p. 127–146, doi:10.1017/S0022112078002505.

Phillips, C.B., Masteller, C.C., Blaylock, J., Van Iwaarden, F., and Johnson, J.P.L., 2024, Variability in River Width Reveals Climatic Influence on Channel Geometry: Geophysical Research Letters, v. 51, p. e2024GL111789, doi:10.1029/2024GL111789.

Phillips, C.B., Masteller, C.C., Slater, L.J., Dunne, K.B.J., Francalanci, S., and Lanzoni, S., 2022, Threshold constraints on the size, shape and stability of alluvial rivers: Nature Reviews Earth & Environment, p. 1–14, doi:10.1038/s43017-022-00282-z.

Prancevic, J.P., and Lamb, M.P., 2015, Unraveling bed slope from relative roughness in initial sediment motion: Relative roughness and incipient motion: Journal of Geophysical Research: Earth Surface, v. 120, p. 474–489, doi:10.1002/2014JF003323.

Shields, A., 1936, Application of similarity principles and turbulence research to bed-load movement:, https://resolver.caltech.edu/CaltechKHR:HydroLabpub167 (accessed January 2021).

Sklar, L.S., and Dietrich, W.E., 2004, A mechanistic model for river incision into bedrock by saltating bed load: Water Resources Research, v. 40, doi:10.1029/2003WR002496.

Syvitski, J.P.M., Vörösmarty, C.J., Kettner, A.J., and Green, P., 2005, Impact of humans on the flux of terrestrial sediment to the global coastal ocean: Science, v. 308, p. 376–380, doi:10.1126/science.1109454.

Turowski, J.M., Yager, E.M., Badoux, A., Rickenmann, D., and Molnar, P., 2009, The impact of exceptional events on erosion, bedload transport and channel stability in a step-pool channel: Earth Surface Processes and Landforms, v. 34, p. 1661–1673, doi:10.1002/esp.1855.

Whitfield, D., Baynes, E.R.C., Hodge, R.A., Rice, S.P., and Yager, E.M., 2025, The Influence of Gravel-Bed Structure on Grain Mobility Thresholds: Comparison of Force-Balance Approaches: Journal of Geophysical Research: Earth Surface, v. 130, p. e2025JF008333, doi:10.1029/2025JF008333.

Wong, M., and Parker, G., 2006, Reanalysis and Correction of Bed-Load Relation of Meyer-Peter and Müller Using Their Own Database: Journal of Hydraulic Engineering, v. 132, p. 1159–1168, doi:10.1061/(asce)0733-9429(2006)132:11(1159).

Yager, E.M., Schmeeckle, M.W., and Badoux, A., 2018, Resistance Is Not Futile: Grain Resistance Controls on Observed Critical Shields Stress Variations: Journal of Geophysical Research: Earth Surface, v. 123, p. 3308–3322, doi:https://doi.org/10.1029/2018JF004817.

Yager, E.M., Turowski, J.M., Rickenmann, D., and McArdell, B.W., 2012, Sediment supply, grain protrusion, and bedload transport in mountain streams: Geophysical Research Letters, v. 39.

FIGURE CAPTIONS

Figure 1. A) sediment transport rating curves; B) Estimates of τ^*_{ref} with channel slope; error bars represent the 75% confidence interval.

Figure 2. Normalized sediment flux, q_{s_n}, with conditioning time for each experimental slope and data from Masteller and Finnegan (2017) with best-fit power laws.

Figure 3. Riverbed strengthening exponent, ζ, as a function of slope. Error bars denote ±1 standard deviation uncertainty associated with the power-law fits used to estimate ζ.

[1]Supplemental Material. Expanded methods description and experimental data. Please visit https://doi.org/10.1130/XXXX to access the supplemental material, and contact editing@geosociety.org with any questions.

GSA Data Repository
Supplemental Information

Slope-dependent riverbed strengthening and the evolution of the threshold for motion in gravel-bed rivers

Robert Kostynick[1], Julia Prata[1], Jesse Bower[2], and Claire Masteller[1]
[1]Earth, Environmental, and Planetary Sciences, Washington University in St. Louis, St. Louis, MO, USA
[2]Department of Civil & Environmental Engineering, Utah State University, Logan, UT, USA

S1. Sediment transport rating curves, estimation of reference Shields stress, and hydraulic scaling

At each experimental slope, a sediment transport rating curve was constructed for a range of flow depths. Flow depths were adjusted between each experimental run by varying the frequency of an adjustable pump drive with a frequency precision of 0.1 Hz. Each rating curve trial had a duration of 3 minutes, during which sediment transport out of the flume was caught in a downstream basket. Flow depths were measured at one upstream, central, and downstream position along the flume using a ruler. At the end of each run, sediment transported out of the flume was weighed, providing a total sediment flux over each 3-minute trial.

Flow depth at a given pump frequency decreases with increasing slope for a given transport condition, such that the range of stable flow depths that could be explored became progressively narrower at steeper slopes. Because of the multiplicative effect of slope on shear stress, this compression in flow depth still produced a wider range of shear stresses even over a smaller range of flow depths and associated pump frequencies. At the steepest slopes, experiments were additionally limited by episodic bed failure, which constrained the number of runs that could be conducted. As a result, rating curves at higher slopes are based on a more limited range of flow conditions and therefore carry greater uncertainty.

To convert average flow depths for each experiment to dimensionless Shields stress, τ^*, we used

$$\tau^* = \frac{\rho g R S}{(\rho_s - \rho) g D_{50}} \quad (1).$$

Where ρ and $\rho_s$are water and sediment density, respectively, with units kg/m3, g is acceleration due to gravity (m/s2), R is the hydraulic radius (m), S is channel slope (m/m), and D_{50} is median grain size (m). Slope and hydraulic radius vary for each experimental run (See Supplementary Dataset), all other parameters are held constant (Table S1).

Table S1. Parameter values for Shields stress calculation

Parameter	Value
water density, ρ	1000 kg/m3
sediment density, ρ_s	2650 kg/m3
gravity, g	9.81 m/s2
median grain size, D_{50}	0.074 m

Following conversion from flow depth to Shields stress, we convert total flux to dimensionless transport rate, defined as

$$q_s^* = \frac{q_s}{\sqrt{\frac{\rho_s - \rho}{\rho} g {D_{50}}^3}} \qquad (2),$$

where q_s is the dimensional flux rate (kg/m/s), calculated as the total bedload flux divided by the run time and the flume width. To estimate τ_{ref}^*, we fit a power law to each slope-specific rating curve. We then use these best-fit power law relationships to estimate τ_{ref}^* at a reference transport rate $q_s^* = 0.08$. We selected this reference transport rate to ensure that two data points from each rating curve experiment fell below this reference rate. We note that following this procedure, the selection of a lower reference transport rate would compress the range of τ_{ref}^*, but would not meaningfully change the form or goodness-of-fit between τ_{ref}^* and slope.

We note that we completed this procedure at 5 slopes, S = 5, 10, 25, 50, and 70 mm/m. However, we did include conditioning experiments at S = 10 mm/m, instead incorporating previous experiments from Masteller and Finnegan (2017) from a similar slope. Nevertheless, the additional rating curve helps to inform the relationship between slope and τ_{ref}^*, as well as the hydraulic scaling used in our low flow conditioning experiments, so we opt to include it here.

Based on τ_{ref}^* estimates, flow depths and pump frequencies were selected to target approximately $0.75\tau_{ref}^*$and $1.2\tau_{ref}^*$, while accounting for uncertainty in the rating-curve estimates of τ_{ref}^*. Some trial and error was required to ensure that the experiments captured conditioning and sediment-transporting flow conditions and prevent bed failure at steep slopes. Consistent with this design, little to no sediment transport was observed during conditioning phases.

S2. Low flow conditioning experiments

Across all experiments, sediment flux decreases systematically with increasing conditioning time. Three of the four experimental slopes (S = 0.025–0.070 m/m) occupy a similar range of sediment flux values and exhibit comparable declines in flux with conditioning time. In contrast, the lowest slope experiment (S = 0.005 m/m) shows

systematically lower flux values, which likely reflects uncertainty in the transport flow associated with the rating-curve-derived hydraulic scaling. Data from Masteller and Finnegan (2017) plot above the new experimental data. This offset is not unexpected, as those experiments were conducted at a different facility and slope effects were not explicitly accounted for when estimating the hydraulic scaling between conditioning and transport phases. These offsets are captured by the coefficients of the best-fit power laws, whereas the riverbed strengthening exponents, which quantify the rate of flux reduction with conditioning time, vary systematically with slope.

To facilitate comparison across slopes and with previous experiments from Masteller and Finnegan (2017) (S = 8 mm/m), q_s was normalized using the data-derived regression for each experiment. Specifically, flux values were rescaled by the flux predicted by the best-fit regression at $t = 1$, effectively normalizing by the coefficient of each regression.

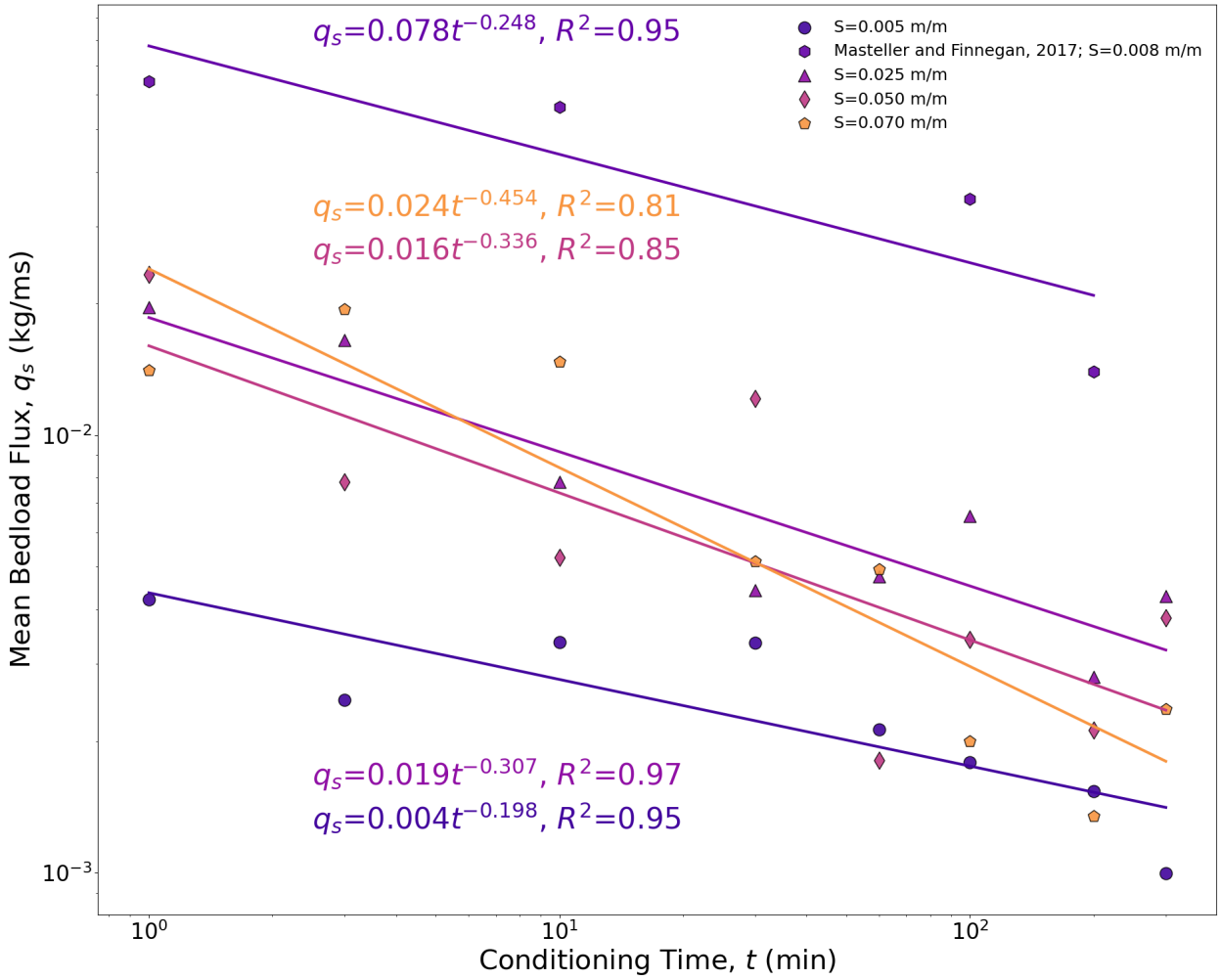

Figure S1. Mean bedload flux measurements as a function of conditioning time with best-fit power laws and goodness-of-fit metrics.

Summary of Supporting Dataset

We provide the experimental dataset supporting this contribution as a .xlsx file. In the provided file we provide the experimental data from rating curve construction, estimates of τ^*_{ref}, antecedent low flow experimental data, and ζ values.

Table 1. Rating Curve Data.

Slope, S (m/m)	Average Flow Depth, h (m)	Hydraulic Radius, R (m)	Shields Stress, Tau*	Run Time (s)	Total Sediment Flux, Qs_total (kg)	Sediment Flux, qs (kg/m/s)	Dimensionless sediment flux, qs*
0.005	0.023	0.020	0.008	180	4.200E-04	5.819E-06	2.272E-03
0.005	0.035	0.030	0.012	180	8.530E-03	1.182E-04	4.614E-02
0.005	0.043	0.035	0.014	180	1.512E-01	2.095E-03	8.181E-01
0.005	0.051	0.040	0.017	180	2.441E-01	3.382E-03	1.321E+00
0.005	0.059	0.045	0.019	180	2.612E-01	3.618E-03	1.413E+00
0.005	0.066	0.050	0.020	180	6.682E-01	9.257E-03	3.614E+00
0.005	0.075	0.055	0.022	180	1.268E+00	1.757E-02	6.859E+00
0.005	0.073	0.054	0.022	180	9.157E-01	1.269E-02	4.954E+00
0.005	0.079	0.056	0.023	180	1.997E+00	2.766E-02	1.080E+01
0.01	0.015	0.014	0.011	180	9.700E-04	1.344E-05	5.247E-03
0.01	0.024	0.021	0.017	180	1.459E-02	2.021E-04	7.892E-02
0.01	0.035	0.030	0.025	180	8.056E-02	1.116E-03	4.358E-01
0.01	0.044	0.036	0.030	180	2.160E-01	2.993E-03	1.169E+00
0.01	0.056	0.044	0.036	180	5.242E-01	7.263E-03	2.836E+00
0.01	0.059	0.045	0.037	180	1.026E+00	1.421E-02	5.548E+00
0.025	0.006	0.006	0.013	180	6.000E-05	8.313E-07	1.257E-02
0.025	0.015	0.014	0.029	180	5.470E-03	7.578E-05	2.857E-02
0.025	0.018	0.017	0.034	180	2.440E-02	3.380E-04	3.439E-02
0.025	0.023	0.020	0.042	180	4.256E-02	5.896E-04	4.170E-02
0.025	0.028	0.025	0.050	180	1.020E-01	1.412E-03	5.030E-02
0.025	0.029	0.026	0.052	180	1.215E-01	1.683E-03	5.239E-02
0.025	0.025	0.022	0.046	180	4.357E-01	6.036E-03	4.551E-02
0.025	0.028	0.025	0.051	180	3.068E-01	4.250E-03	5.083E-02
0.025	0.032	0.028	0.057	180	4.154E-01	5.755E-03	5.650E-02
0.025	0.034	0.029	0.060	180	2.112E-01	2.926E-03	6.002E-02
0.025	0.032	0.028	0.057	180	1.813E-01	2.511E-03	5.650E-02
0.025	0.036	0.030	0.062	180	4.222E-01	5.849E-03	6.200E-02
0.025	0.033	0.028	0.058	180	9.341E-01	1.294E-02	5.751E-02
0.025	0.035	0.030	0.062	180	8.874E-01	1.229E-02	6.151E-02
0.025	0.040	0.034	0.069	180	3.537E+00	4.901E-02	6.875E-02
0.05	0.005	0.005	0.021	180	7.000E-05	9.698E-07	3.787E-04
0.05	0.011	0.011	0.044	180	6.540E-03	9.061E-05	3.538E-02
0.05	0.013	0.012	0.050	180	9.263E-02	1.283E-03	5.011E-01
0.05	0.018	0.017	0.068	180	2.561E-01	3.548E-03	1.385E+00

0.05	0.021	0.019	0.077	180	1.488E-01	2.061E-03	8.047E-01
0.05	0.021	0.019	0.079	180	4.693E-01	6.502E-03	2.539E+00
0.07	0.005	0.005	0.028	180	8.000E-05	1.108E-06	4.328E-04
0.07	0.009	0.009	0.049	180	2.150E-03	2.979E-05	1.163E-02
0.07	0.018	0.017	0.095	180	1.881E-01	2.606E-03	1.018E+00
0.07	0.020	0.018	0.106	180	1.398E-01	1.937E-03	7.564E-01
0.07	0.019	0.017	0.099	180	1.139E+00	1.578E-02	6.160E+00

Table 2. Reference Shields Stress Estimates

Slope	Reference Shields Stress
0.005	0.012
0.01	0.018
0.025	0.032
0.05	0.046
0.07	0.063

Table 3. Low Flow Conditioning Experimental Data

Slope	Conditioning Time	Average bedload flux, kg/m/s	Normalized Bedload Flux	
0.005	1	0.004	0.966	
0.005	3	0.002	0.570	
0.005	10	0.003	0.771	
0.005	30	0.003	0.770	
0.005	60	0.002	0.488	
0.005	100	0.002	0.410	
0.005	200	0.002	0.352	
0.005	300	0.001	0.229	
0.008	1	0.065	0.831	Masteller and Finnegan, 2017
0.008	10	0.056	0.726	Masteller and Finnegan, 2017
0.008	100	0.035	0.447	Masteller and Finnegan, 2017
0.008	200	0.014	0.180	Masteller and Finnegan, 2017
0.025	1	0.020	1.056	
0.025	3	0.017	0.888	
0.025	10	0.008	0.422	
0.025	30	0.004	0.238	
0.025	60	0.005	0.256	
0.025	100	0.007	0.352	
0.025	200	0.003	0.151	
0.025	300	0.004	0.231	
0.050	1	0.023	1.458	
0.050	3	0.008	0.489	
0.050	10	0.005	0.328	
0.050	30	0.012	0.757	
0.050	60	0.002	0.113	
0.050	100	0.003	0.213	
0.050	200	0.002	0.132	
0.050	300	0.004	0.239	
0.070	1	0.014	0.585	
0.070	3	0.019	0.809	
0.070	10	0.015	0.613	
0.070	30	0.005	0.214	
0.070	60	0.005	0.205	
0.070	100	0.002	0.083	
0.070	200	0.001	0.056	
0.070	300	0.002	0.098	

Table 4. Strengthening Exponents

Slope	Strengthening exponent
0.005	0.198
0.008	0.248
0.025	0.307
0.05	0.336
0.07	0.454